Astron. Astrophys. 363, 1029–1039 (2000)

ASTRONOMY AND ASTROPHYSICS

Time-resolved optical studies and Doppler imaging of the eclipsing dwarf nova V893 Scorpii⋆

K. Matsumoto[1], **R.E. Mennickent**[2], **and T. Kato**[1]

[1] Kyoto University, Faculty of Science, Department of Astronomy, Sakyo-ku, Kyoto 606-8502, Japan (katsura@kusastro.kyoto-u.ac.jp; tkato@kusastro.kyoto-u.ac.jp)
[2] Universidad de Concepción, Departamento de Física, Casilla 160-C, Concepción, Chile (rmennick@stars.cfm.udec.cl)

Received 2 September 1999 / Accepted 21 September 2000

Abstract. We present time-resolved optical spectroscopic and photometric observations of the re-discovered dwarf nova V893 Sco. The orbital period of $0^{\rm d}.07610(3)$ derived from the radial velocity and equivalent width variations of the Hα emission line is confirmed. The photometric light curves clearly show the eclipse of the accretion disk. A mass of the white dwarf $\sim$0.5–0.6 $M_\odot$ is derived from the orbital amplitude $K_1 = 86 \pm 11$ km s^{-1} and the eclipse constraint. The mass ratio is likely small enough to make V893 Sco an SU UMa-type dwarf nova, though this object has shown only normal outbursts in its light curve. Time-resolved Doppler maps for the emission lines show two isolated Hα emission regions, which are associated with a strong hot spot and the irradiated secondary star.

Key words: accretion, accretion disks – stars: binaries: close – stars: individual: V893 Sco – stars: novae, cataclysmic variables

1. Introduction

Cataclysmic variables (CVs) are close binary systems consisting of a mass-accreting white dwarf and a mass donor secondary star which fills its Roche lobe. The accreting matter falls in a ballistic trajectory and can form an accretion disk around the white dwarf. Three subclasses are identified in non-magnetic CVs: novae, novalike stars, and dwarf novae. Dwarf novae display quasi-periodic outbursts that are believed to be caused by a thermal instability of the accretion disk (for a review see Warner 1995).

V893 Sco was originally discovered by Satyvoldiev (1972) as a suspected CV, but remained uncatalogued and unnoticed until 1998, when Katsumi Haseda, an amateur astronomer, re-discovered it in his photographic plates. This star was re-identified by Kato et al. (1998), who also utilized the fact that the object was detected by ROSAT as RXS 161516.2−283712 ($\alpha = 16^{\rm h}\,15^{\rm m}\,15\overset{\rm s}{.}15, \delta = -28^\circ\,37'\,30\overset{''}{.}1$ (J2000)).

The photometric behavior followed by Satyvoldiev (1982) was suggestive of repetitive dwarf nova outbursts. The object is usually around 13–14 mag in V-band and shows outbursts with an amplitude of around 2 mag, according to the current VSNET database[1]. Thorstensen (1999) obtained optical spectra of this object, and reported an orbital period of $0^{\rm d}.0760$ with a possible one-day alias of $0^{\rm d}.0822$, i.e., just below the 2–3 h period "gap". The photometric study by Bruch et al. (2000) revealed shallow eclipses and the irregular flickering dominating the optical light curve.

We report in this paper our time-resolved spectroscopic and photometric observations of this object obtained in order to follow its orbital behavior and resolve its nature. The fact that the spectra are densely sampled in orbital phase permits us to perform a Doppler tomographic analysis of the emission lines (see e.g., Marsh & Horne 1988; Kaitchuck et al. 1994 for more information).

2. Observations and data reductions

2.1. Spectroscopy

The spectroscopic observations were made on seven nights in April and May 1998 with the ESO 3.5-m NTT at La Silla. The observing time was divided into two runs: the first on April 17–20 and the second on May 29–31. The EMMI spectrograph in its red medium dispersion mode (REMD), grating #8, and the red arm CCD camera #36 were used. This setup and the slit width of one arcsecond yielded a spectral resolution of 2.5 Å, and a spectral range of 4450–7025 Å. A spectrum with the grating #13 was additionally taken in the first night, providing a wider wavelength range of 4188–9623 Å. He-Ar comparison spectra were taken in intervals of typically 30 minutes. For the scientific exposures, 120–300 s integration times were used. The other calibration frames (bias and flat images) were taken during the daytime. A summary of the observing log is given in Table 1. Since the three frames on April 17 were only taken for test purposes, they were not used for detailed analyses but only for obtaining a general view of the spectral features.

Send offprint requests to: K. Matsumoto

⋆ Based on observations obtained at ESO La Silla Observatory (ESO Proposal 61.D-0395)

[1] http://www.kusastro.kyoto-u.ac.jp/vsnet/LCs/index/scov893.html

Table 1. An observing log of the spectroscopy.

UT Date (1998)		HJD (−2450000)	number of object frames	exposure time
April	17	921.8952–921.9192	3*	300s
	18	922.6304–922.9128	86	120–180s
	19	923.6278–923.9332	50	180–300s
	20	924.6185–924.9310	62	120–300s
May	29	963.6294–963.9131	49	180s
	30	964.5980–964.6590	20	180s
	31	965.7620–965.9075	44	180s

* including one snapshot with the grating #13 of the NTT REMD (Fig. 2)

Table 2. An observing log of the Kyoto photometry.

UT Date (1999)		HJD (−2450000)	Number of object frames
April	29	1298.1785–1298.3053	262
	30	1299.1406–1299.3071	349
May	1	1300.1387–1300.3101	233
	12	1311.2164–1311.2994	152
	13	1312.1496–1312.2889	256
	20	1319.0787–1319.2747	460

The data reduction was performed in a standard manner using the IRAF[2] software. Wavelength calibrations with typical rms of about 0.4 Å were obtained using the He-Ar comparison spectra. Flux calibrations were performed with EG 274 as a standard star before the spectra were finally normalized to the continuum. Velocities relative to the Local Standard of Rest were used for the analyses presented in this paper.

2.2. Photometry

We measured integrated fluxes in the spectra of the object and a comparison star placed in the same slit as the variable during the second NTT run (1998 May 29–31). The comparison star is 26.8 arcseconds South and 11.6 arcseconds West of the object. After rejecting spectra with poor S/N due to bad slit centering, we obtained the relative brightnesses providing a set of "slit differential magnitudes".

We additionally obtained time-resolved CCD photometric observations in order to better define the photometric characteristics of the object. The photometric observations were done using an unfiltered KAF-0400 CCD camera (SBIG ST-7) attached to a 25-cm Schmidt-Cassegrain telescope (Meade LX200) on the rooftop of the Department of Astronomy, Kyoto University, during April and May 1999. The exposure time was set to 30 s. The frames were dark-subtracted, flat-fielded, and analyzed using a Java™-based aperture and PSF photometry package developed by one of the authors (T.K.). We determined the relative magnitudes of the object using the local comparison star GSC 6805.837 (V = 12.893, $B-V$ = 1.772), whose constancy was confirmed by comparison with GSC 6805.1166 (V = 14.602, $B-V$ = 0.838). A heliocentric time correction was applied before the analysis. The 1999 Kyoto run is summarized in Table 2.

[2] IRAF is distributed by the National Optical Astronomy Observatories, which are operated by the Association of Universities for Research in Astronomy, Inc., under cooperative agreement with the National Science Foundation

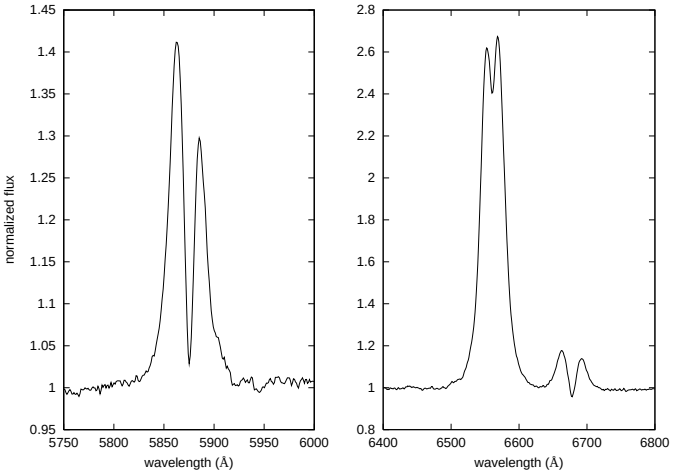

Fig. 1. He I λ5876 (left) and Hα (right) profiles from the averaged spectrum of V893 Sco. The flux is normalized by the continuum level.

3. Results – spectroscopy

3.1. Optical spectral features

The optical spectrum of the object is characterized by emission lines of the Balmer series and neutral and ionized helium on a blue continuum (Figs. 1, 2). The He II λ4686 emission line is relatively weak but present as also pointed out by Thorstensen (1999). The O I λ6345 emission line is possibly detected in the averaged spectrum. The emission at Hγ, He I λ7065, O I λ7772, He II λ8236, and Paschen lines is also seen in the snapshot taken with grating #13 (Fig. 2). The O I λ7772 is in absorption, suggesting a nearly edge-on accretion disk and a high inclination angle of the system (Smith 1990). The spectra as a whole have the general features seen in those of dwarf novae during quiescence.

All the emission lines seen in the spectrum have double-peaked profiles, suggesting these lines are produced in the accretion disk. Relatively strong absorption cores below the continuum level appear for the neutral helium lines, while those of the He II λ4686 are relatively weak. The depth of the self-absorption has no dependence on spectroscopic phase. No absorption features from the secondary are seen.

3.2. Radial velocities and the orbital period

To search for the orbital period of the object, radial velocities were obtained for the Hα emission line using the convolved double-Gaussian method (Schneider & Young 1980; Shafter 1983; Horne et al. 1986) and various separations between 25 and

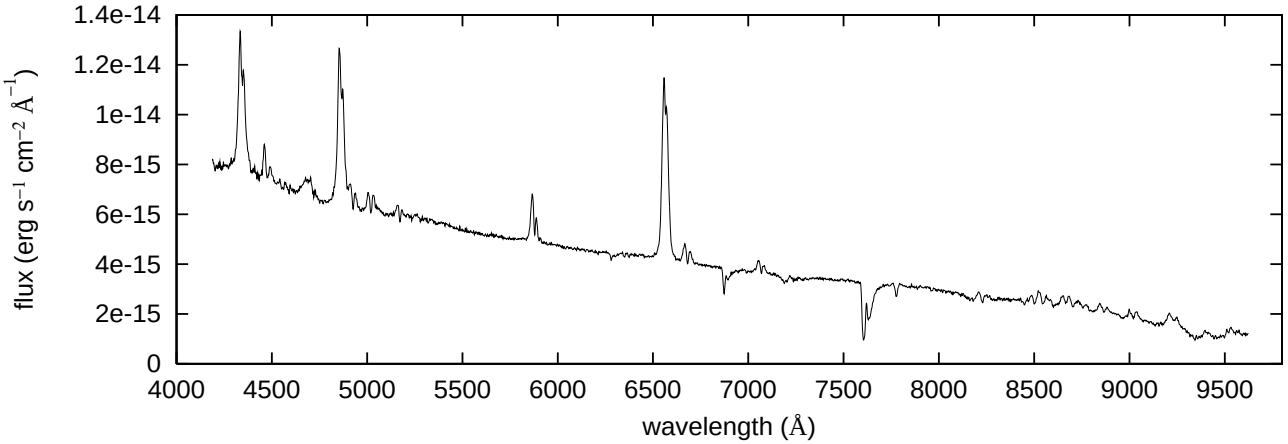

Fig. 2. The spectrum of V893 Sco taken on 1998 April 17.

110 Å for the double-peaked convolution profile. A sinusoidal fit to the radial velocity curves for each separation was obtained using the expression

$$v_{\rm RV} = A\sin(2\pi\Phi) + B\cos(2\pi\Phi) + \gamma, \quad (1)$$

where γ and Φ are the systemic velocity and the spectroscopic phase shift, respectively, and A and B are coefficients for the semi-amplitude $K = \sqrt{A^2 + B^2}$. The diagnostic parameter σ_K/K was computed for each separation (Fig. 3; see e.g., Shafter et al. 1986), and has a minimum for separations around 50 Å. This gives a 0.07610 d periodicity as the strongest signal in the radial velocity curve. The final periodogram is shown in Fig. 4. Thorstensen (1999)'s alias of 0.08220 d can also be seen. However, we regard the $0\overset{\rm d}{.}07610$ period as the orbital period, being consistent with the result of Thorstensen (1999) and the photometrically determined period by Bruch et al. (2000).

The spectroscopic ephemeris of the strongest radial velocity signal (corresponding to the change of radial velocity from positive to negative relative to the systemic velocity) is

$$\mathrm{HJD} = 2450922.62015(53) + 0.07610(3)E. \quad (2)$$

The radial motion of the white dwarf was investigated by following the velocity variations of the wings of Hα line using the same double-Gaussian method ($FWHM = 8$ Å). The profile of the emission line suggests that the radial velocity variation at 80–90 Å separation is a better tracer of the orbital motion of the white dwarf: given the $0\overset{\rm d}{.}07610$ orbital period, the diagnostic diagram (Fig. 3) shows a rapid increase in σ_K/K for separations larger than 90 Å. We adopt the orbital parameters associated with the separation before the noise starts to dominate, i.e., 85 Å: $K_1 = 86 \pm 11$ km s^{-1}; $\gamma = -10.7 \pm 5.3$ km s^{-1}; and $\Delta\Phi = 0.075 \pm 0.02$. The radial velocity curve sampled for the 85 Å separation is shown folded on the orbital period in Fig. 5.

We find a relatively larger radial velocity scatter around spectroscopic phase $\Phi_{\rm spec} \sim 0.8$, which indicates a rotational disturbance. This feature is most clearly seen in a velocity curve sampled with the minimum σ_K/K of the 50 Å separation: in Fig. 5, the lower S/N of the sampling at the wider separation weakens the feature.

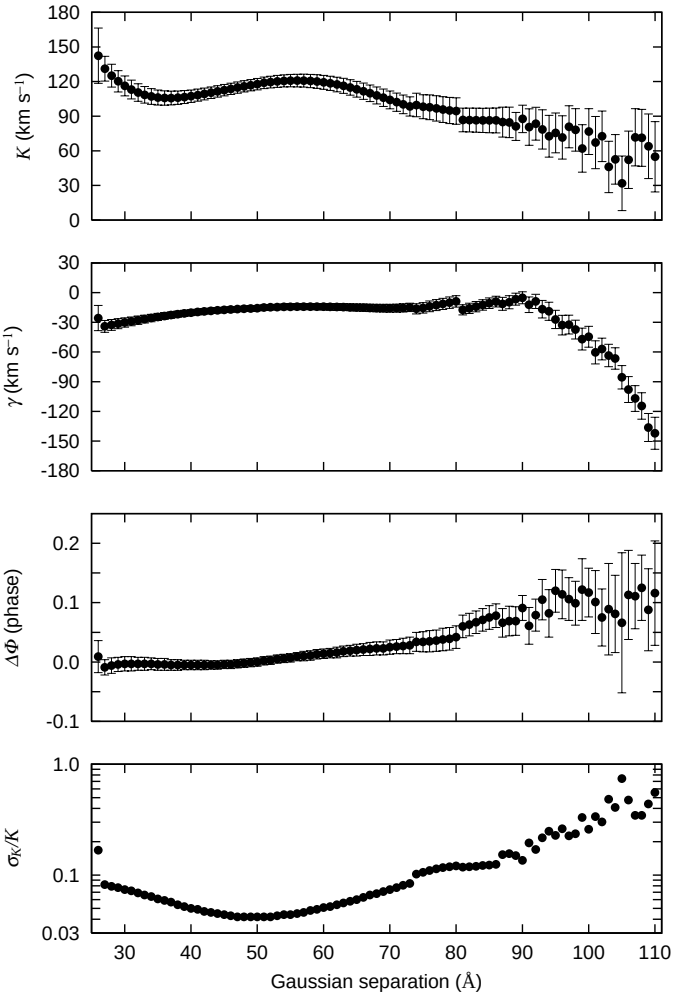

Fig. 3. The diagnostic diagram for Hα radial velocity measurements.

3.3. Equivalent widths

The Balmer emission lines dominate the spectrum and are characterized by large equivalent widths. The values are typically about 70 Å and 40 Å for Hα and Hβ, respectively, while those of the helium lines are relatively weaker with about 13 Å for

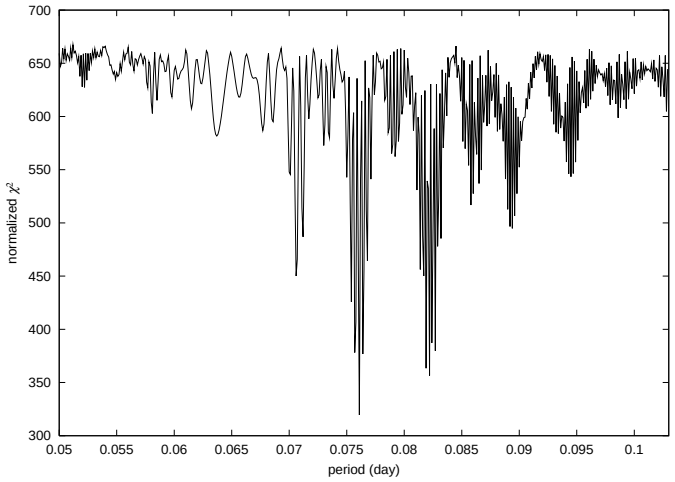

Fig. 4. The periodogram for the radial velocity of Hα.

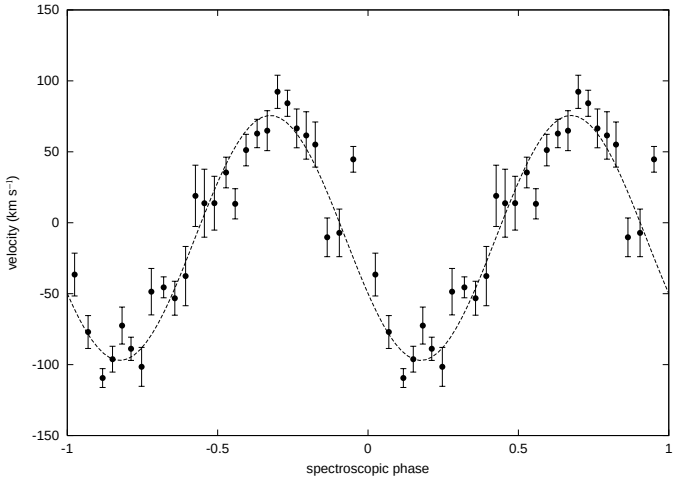

Fig. 5. The best-fit velocity curve of the Hα wings (85 Å separation) folded with the $0^{\rm d}.07610$ orbital period. The data are averages of each 10 successive points. Note that the spectroscopic phase is based on the ephemeris given in Eq. (1) (50 Å separation). The zero-crossing point is ~ 0.07 phase shifted from that based on Eq. (1). The phase is repeated twice for clarity.

the He I λ5876 line, and about 6 Å for the other neutral or ionized helium lines and the Fe II λ5169 line. Fig. 6 shows that the equivalent width has a weak dependence on the orbital period. On May 31, our last night of spectroscopy, an outburst started according to the VSNET database[3]. Because of the outburst, the strengths of the all lines suddenly decreased: the equivalent widths of the Hα and Hβ were respectively about 25 Å and 5 Å, and those for the other lines were around 1 or 2 Å.

4. Results – photometry

Fig. 7 shows the light curve derived from the slit magnitudes in the 1998 NTT run, folded by the $0^{\rm d}.07610$ orbital period after removing the nightly brightening tendency due to the pre-

[3] http://www.kusastro.kyoto-u.ac.jp/vsnet/etc/searchobs.cgi?text=SCOV893

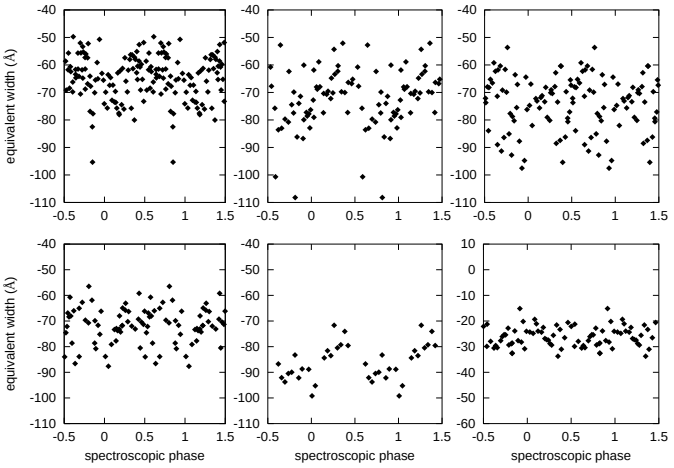

Fig. 6. The equivalent width of Hα folded by the orbital period and plotted for the individual nights (April 18–20 (top) and May 29–31 (bottom) for left to right, respectively).

outburst stage. The rms scatter in the photometry is approximately 0.2 mag, but an eclipse with ~ 0.5 mag depth is detected in the light curve. Details outside eclipse are not so clear, except a possible hump around photometric phase $\Phi_{\rm phot} \sim 0.8$.

The photometric sequence cannot be used to determine the orbital period due to the large scatter of the data. A timing of the eclipse is roughly estimated as HJD = 2450963.781(3) for the data of May 29, corresponding to $\Phi_{\rm spec} \sim 0.88 \pm 0.04$. This ephemeris is consistent with the rotational disturbance seen around $\Phi_{\rm spec} \sim 0.9$ in the folded radial velocity curves. Fig. 8 displays the radial velocity variation of Hα around the eclipse on May 29; the data sets of 50 Å separation are used in order to emphasize timings of rotational disturbances, so note the best-fitted curve is based on the ephemeris given in Eq. (1). The figure indicates that the timing of the eclipse is just coincident with a disturbed point in the radial velocity, and shows the photometric minima $\Phi_{\rm phot} = 0$ shifted from $\Phi_{\rm spec} = 0$.

Fig. 9 shows the light curve of the 1999 Kyoto run folded at the $0^{\rm d}.07610$ orbital period; the bins contain about 30 data each after removing the systematic differences of magnitudes among the individual nights (a post-outburst phase around HJD = 2451311). Due to the low altitude of the object from the observatory, data points at large air mass were excluded. We obtained a photometric minimum at HJD = 2451298.236(2) ($\Phi_{\rm spec} \simeq 0.82 \pm 0.15$). The shape is similar to that of the slit photometry, showing an orbital hump at $\Phi_{\rm phot} \sim 0.8$ and an eclipse with ~ 0.3 mag depth and ~ 0.1 orbital phase width. A possible secondary minimum may be seen around $\Phi_{\rm phot} \sim 0.5$ on the light curve.

5. Discussion

5.1. Phase timings

Fig. 11 and Fig. 13 show the orbital trailed spectra of Hα and He I λ5876 folded with the orbital period along with the corre-

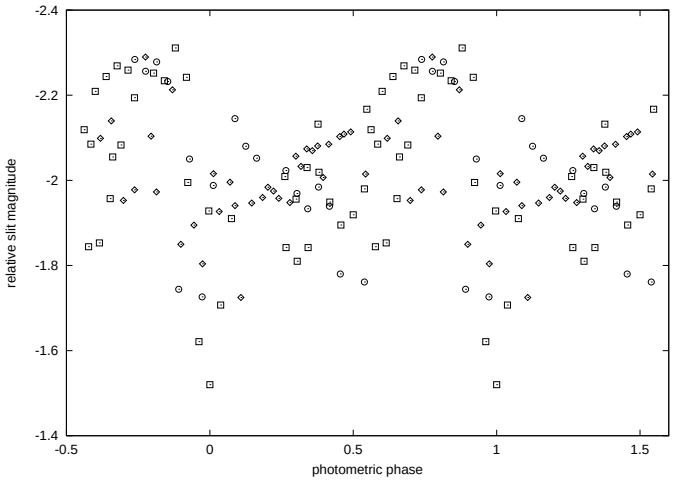

Fig. 7. The light curve by the slit photometry folded by the $0^{\rm d}.07610$ orbital period. The open squares, circles, and diamonds respectively represent the data of May 29, 30, and 31. The zero point of the photometric phase is based on the timing of the eclipse (HJD = 2450963.781).

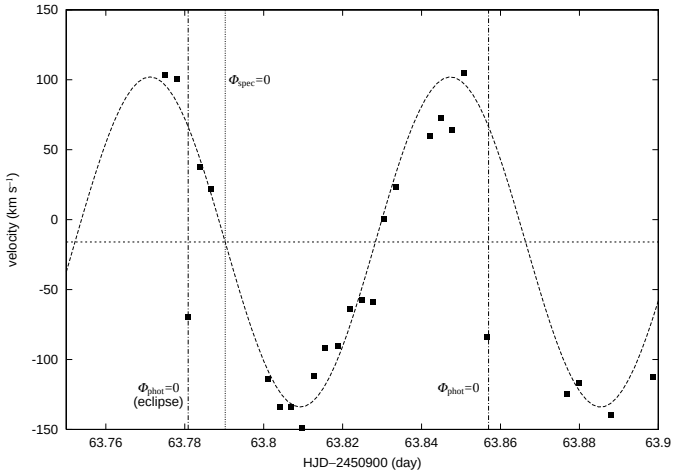

Fig. 8. The radial velocity variation of a part of May 29 (the filled squares). The timings of the spectroscopic and photometric minima are indicated as the vertical dash-dotted and dotted lines, respectively. The long-dashed line represents the fitted sinusoid based on the ephemeris given in Eq. (1), and the horizontal short-dashed line represents the systemic velocity.

sponding Doppler reconstructions (see below)[4]. The phase used here is consistent with the photometric phase expected under the assumption that the photometric phase reflects the orbital phase (i.e., inferior conjunction of the secondary star occurs at $\Phi_{\rm phot} = 0.0$). The spectra of $\Phi_{\rm phot} \sim 0.0 \pm 0.1$ corresponding to the rotational disturbance, whose phasing in the trailed spectra of the individual nights seem to be slightly different within about 0.2 phase were removed prior to mapping, because they possibly affect the results. Each reconstructed spectrum therefore shows voids at the corresponding phases.

[4] The procedures of the mapping were performed using a Doppler tomography tool developed for accretion disks in binary systems by Spruit (1999).

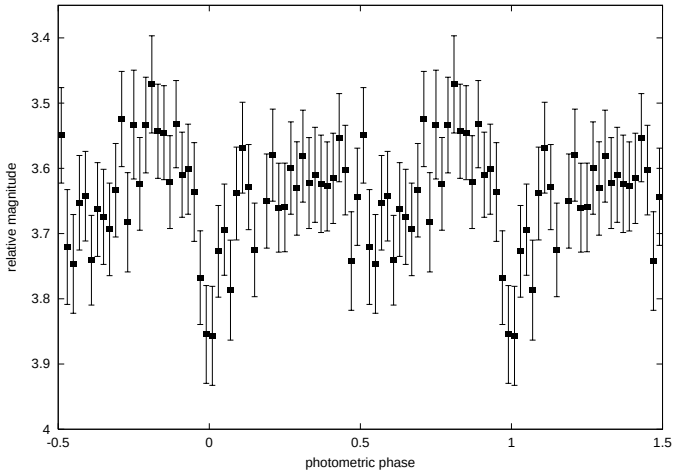

Fig. 9. The photometric light curve of the 1999 Kyoto run folded on the orbital period. The zero point of the photometric phase is based on the timing of the eclipse.

The trailed spectra show both of the double peaks of the emission lines and a clear S-wave modulating independently the global emission pattern with the orbital frequency. These features are the main cause of the orbital variability of the radial velocity corresponded to the spectroscopic ephemeris (Eq. 2). Although weaker, the same phenomenon is also seen in the He I λ5876 emission line (Fig. 13).

The fact that the phases of the rotational disturbance ($\Phi_{\rm spec} \sim 0.9$), the zero-crossing phase of the Hα wings ($\Phi_{\rm spec} = 0.93 \pm 0.02$), and the photometric eclipses ($\Phi_{\rm spec} = 0.88 \pm 0.04$) agree within the errors gives us some confidence that we know the orbital phasing of the binary components (Fig. 5, Fig. 8).

5.2. System parameters

The mass function of the binary system can be derived from the semi-amplitude of radial velocities of the white dwarf K_1 and the orbital period $P_{\rm orb}$:

$$\frac{K_1^3 P_{\rm orb}}{2\pi G} = 0.0051(17)\ M_\odot, \tag{3}$$

where $K_1 = 86 \pm 11$ km s^{-1} and G is the gravitational constant. The mass of the secondary star M_2 can be independently estimated from the empirical relation between M_2 and $P_{\rm orb}$ for main-sequence secondaries of CVs for $1.3 \leq P_{\rm orb}\ ({\rm h}) \leq 9$ (Warner 1995):

$$M_2 \approx 0.065 P_{\rm orb}^{1.25} = 0.14\ M_\odot. \tag{4}$$

The mass function and M_2 determine a relation between a mass of the primary star M_1 and the inclination angle of the binary system (Fig. 10). The relation immediately indicates that M_1 should be less than $\sim 0.7\ M_\odot$ within the errors of K_1 for the object. If $i \geq 70^\circ$ is adopted as a reasonable inclination angle for a system with shallow eclipses (e.g., Fig. 4 of Bruch et al. 2000), we obtain $M_1 \sim 0.5$–$0.6\ M_\odot$ and then a mass ratio $q = M_2/M_1 \sim 0.2$–0.3.

Although no superoutburst has been detected so far for the object, one may anticipate that the object is a member of the SU UMa-type dwarf novae and will show superoutbursts sometime, based on the orbital period just below the period gap. Superoutbursts are characterized by superimposed superhumps during the bright state. Theoretically, superhumps are expected to be caused by a tidal instability of an eccentric accretion disk of the SU UMa stars by an enhanced 3:1 resonance of a rotational velocity at the outer radius of the accretion disk and the orbital motion (Osaki 1989). A mass ratio $q = M_2/M_1 \leq 0.33$ is required for the tidal instability (Whitehurst 1988; Hirose & Osaki 1990; Whitehurst & King 1991). If the expectation of the $\sim 0.5\ M_\odot$ white dwarf is correct, the object should satisfy the criterion.

5.3. Time-resolved Doppler maps

Fig. 12 and Fig. 14 present the two-dimensional Doppler maps of the Hα and He I λ5876 emission lines; the fit converged to a reduced χ^2 of 1.6. A mass accretion stream and a lobe of the secondary star are drawn only for the map of April 18 (top-left) using the $M_1 = 0.52\ \mathrm{M}_\odot$ and the corresponding $i = 70°$.

The dominant features observed in the Hα maps are two isolated blobs on top of the weaker ring-like accretion disk component. The left blob is almost stationary in the Hα and helium maps, indicating that it is the classical hot spot. The right blob, always present in Hα and definitively absent in the helium map, probably arises from the irradiated secondary star.

This emission disappeared on May 31, which indicates that the Hα emission from the irradiated secondary star decreases during the pre-outburst stage. Models of irradiated secondary stars of short period dwarf novae, show the incident flux produces marked changes in the temperature stratification and emitted spectra of the irradiated star (Brett & Smith 1993). Increased irradiation warms the upper layers of the chromosphere, decreasing the temperature gradient. This effect might induce the Balmer lines to change rapidly from emission to strong absorption during outburst (Houdebine et al. 1995).

Even more remarkable are the Doppler maps of the He I λ5876 line; the Hα and He I λ5876 maps show different features. While a significant fraction of the Hα emission comes from low velocity regions, suggesting an origin near the outer accretion disk, the bulk of the helium emission arises from regions of higher velocity, and the outer edge of the accretion disk is invisible in the helium maps, perhaps caused by self absorption of the emission line. On May 31, the He I emission is dominated by four distinct emission regions superimposed upon a ring of emission at $\sim 650\ \mathrm{km\ s^{-1}}$, all located on the trailing edge of the disk.

The component of the irradiated secondary star on the Doppler map of Hα provides us the radial velocity semi-amplitude of the secondary star K_2. Since the emitting region likely represents the irradiated side of the surface, we adopt $K_2 \geq 250\ \mathrm{km\ s^{-1}}$ approximately at the center of mass of the secondary star. Then, we obtain $q = M_2/M_1 = K_1/K_2 \leq 0.3$ and $M_1 \geq 0.4\ M_\odot$. This result is consistent with Fig. 10 within the errors and confirms the estimation of the system parameters given in the previous subsection, indicating that we can observe V893 Sco as a potential SU UMa-type dwarf nova even if there still is no detection of superoutburst.

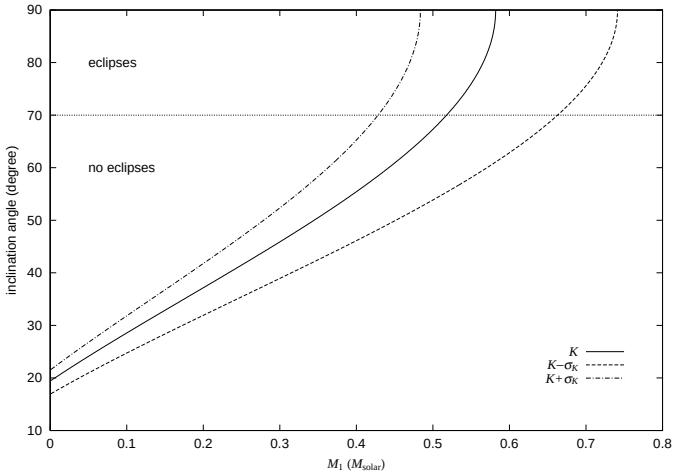

Fig. 10. Expected distributions of the white dwarf mass (M_1, in solar masses) with inclination angle of the binary system assuming $K = 86 \pm 11\ \mathrm{km\ s^{-1}}$ and $M_2 = 0.14\ M_\odot$.

6. Conclusion

The optical spectrum of V893 Sco in quiescence shows broad Balmer and He I emission lines, a weak He II λ4686 emission line, and O I λ7772 in absorption. Based on the radial velocity variations the Hα emission line, we have found an orbital period of 0.07610(3) d. We estimate a white dwarf mass of $\sim$0.5–0.6 $M_\odot$ and mass ratio $q = M_2/M_1 \sim 0.2$–0.3, suggesting that V893 Sco may be an SU UMa-type dwarf nova. Photometric eclipses are seen with a phase consistent with that of the emission line wings and the presence of a rotational disturbance in the S-wave. This coincidence of the timings suggests that eclipses in V893 Sco are of the white dwarf, rather than of a hot spot, by the secondary star. Doppler maps of the Hα line were constructed, showing a stable hot spot and the emission from an irradiated secondary star. The position of the secondary star on the velocity maps confirms the estimated mass ratio satisfying the tidal-instability criterion.

Acknowledgements. The authors would like to express sincere gratitude to the VSNET members for their valuable photometric monitoring, and to the referee F.V. Hessman for his significant comments and corrections. This work is partly supported by the Hayakawa-Yukio Foundation of the Astronomical Society of Japan, and the Research Fellowships of the Japan Society for the Promotion of Science for Young Scientists (K.M.), Fondecyt 1000324, DI UdeC 99.11.28-1 and the National Science Foundation through grant number GF-1002-98 from the Association of Universities for Research in Astronomy, Inc., under NSF Cooperative Agreement No. AST-8947990 (R.M.), and the Grant-in-Aid for Scientific Research (10740095) of the Japanese Ministry of Education, Science, Culture, and Sports (T.K.).

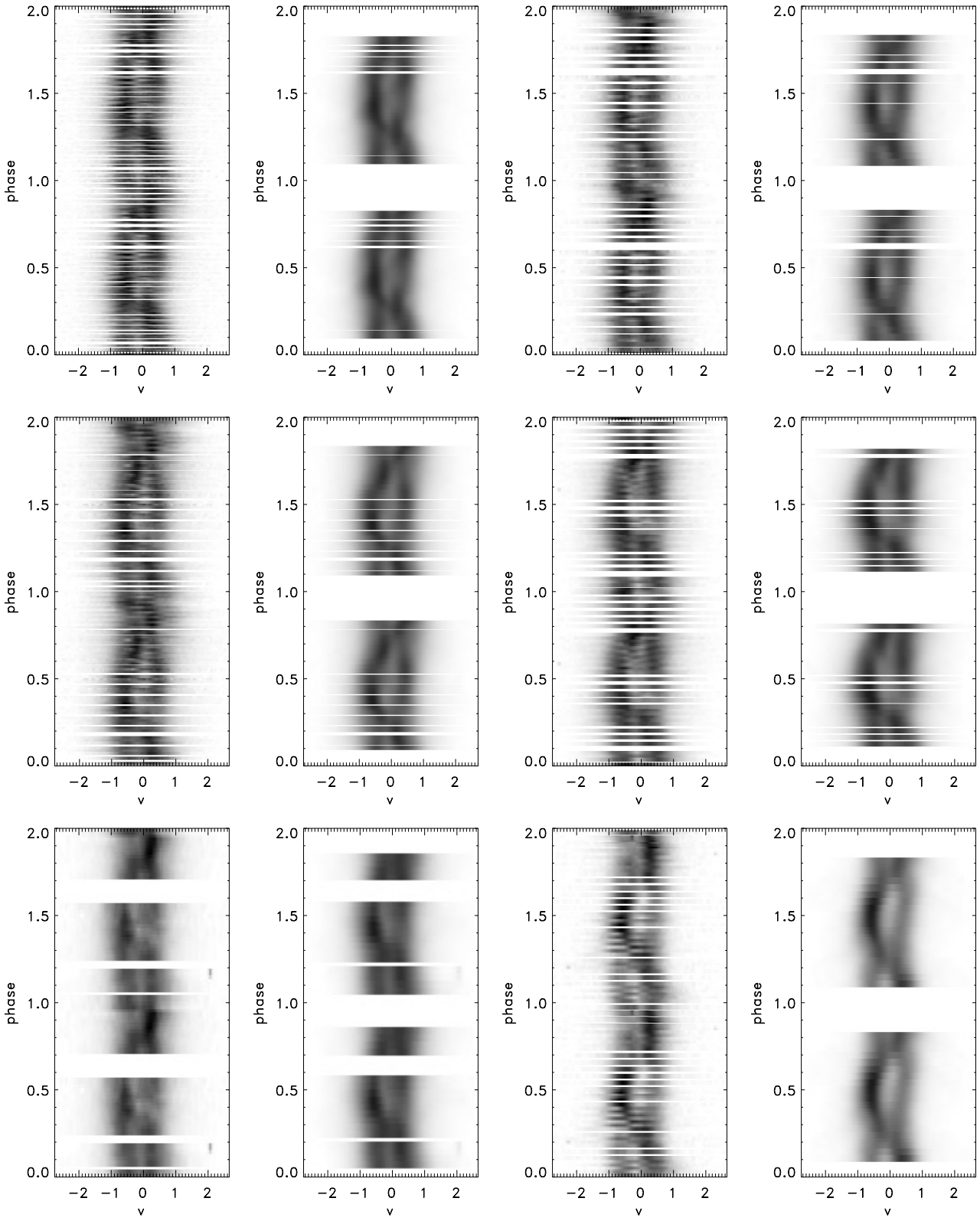

Fig. 11. Observed and reconstructed trailed spectra of Hα for the individual nights (April 18 and 19 (top), April 20 and May 29 (middle), May 30 and 31 (bottom) for left to right, respectively). For each night, two images of the observed (left) and reconstructed (right) spectra are arranged side by side. The vertical axis corresponds to the photometric phase. The rotational disturbance is removed for the reconstructed spectra, i.e., spectra of the phase 0.1–0.8 were used for the mapping ($\Phi = 0.8$–0.9 were also excluded as a preventive measure). The horizontal axis represents the velocity (10^8 cm s^{-1}).

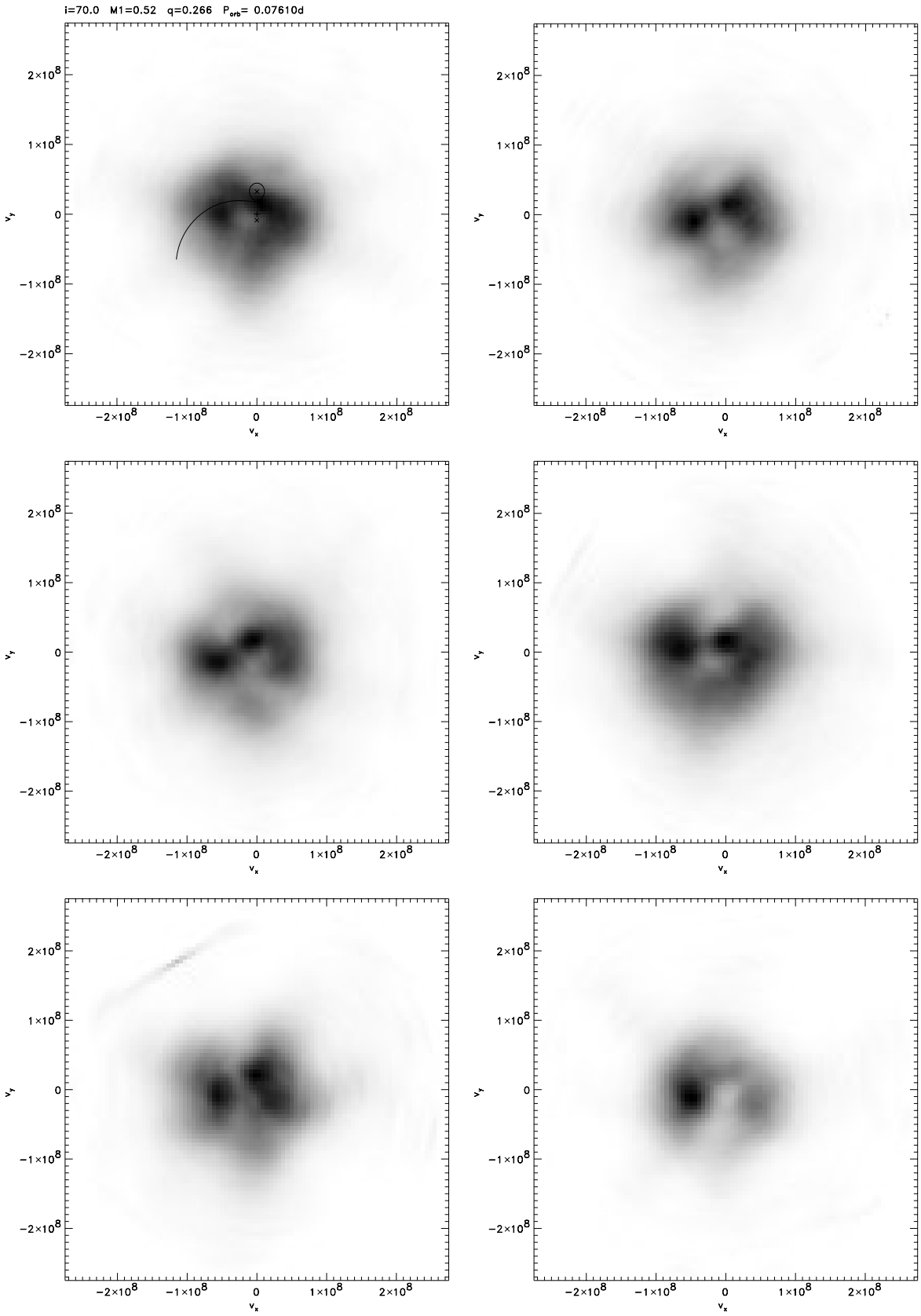

Fig. 12. Doppler maps of Hα (April 18 and 19 (top), April 20 and May 29 (middle), May 30 and 31 (bottom) for left to right, respectively), that is made removing the phase corresponding to the rotational disturbance. The horizontal and vertical axes represent the velocity (cm s^{-1}).

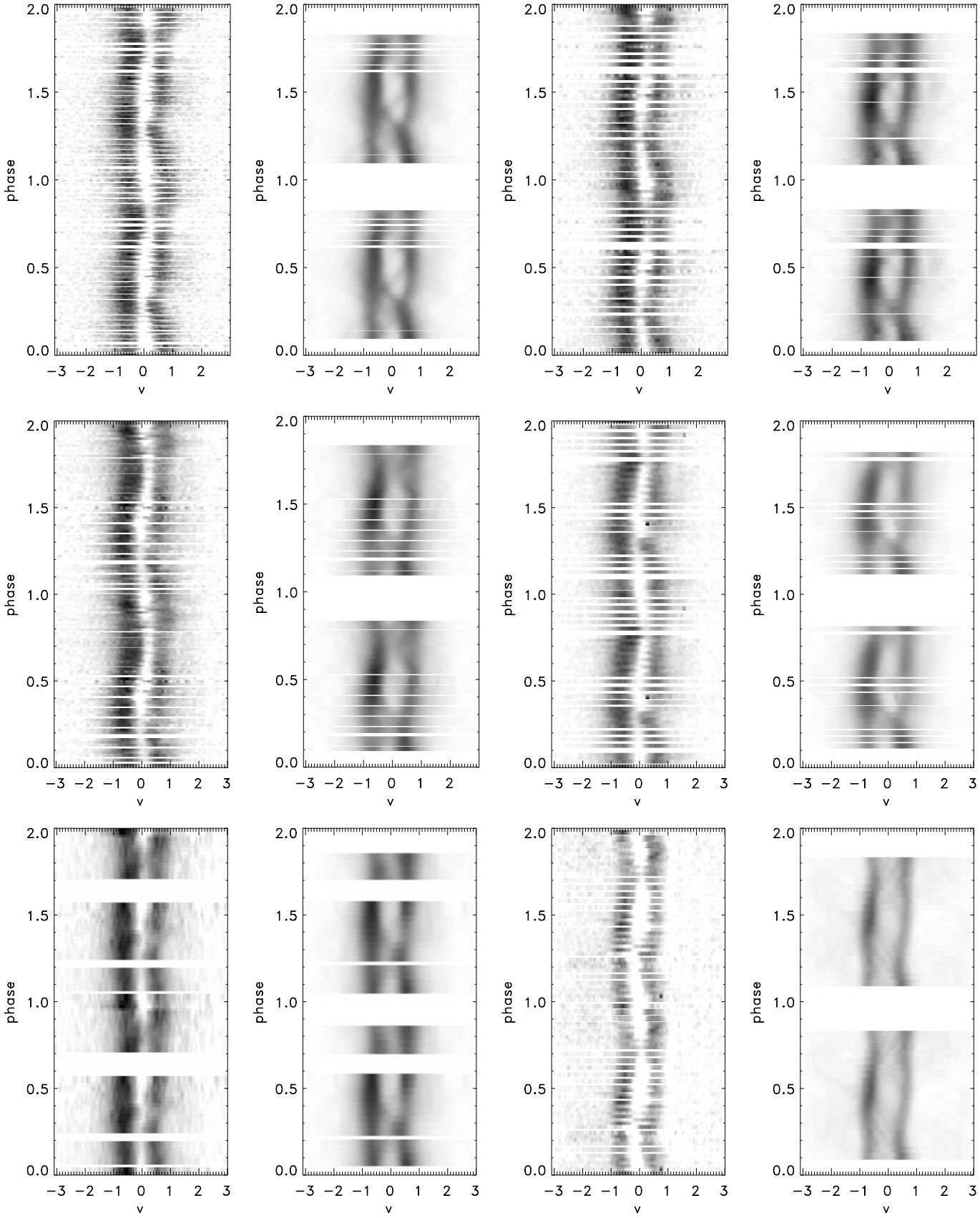

Fig. 13. Trailed spectra of He I λ5876. The arrangement of the figures is same as that of Fig. 11.

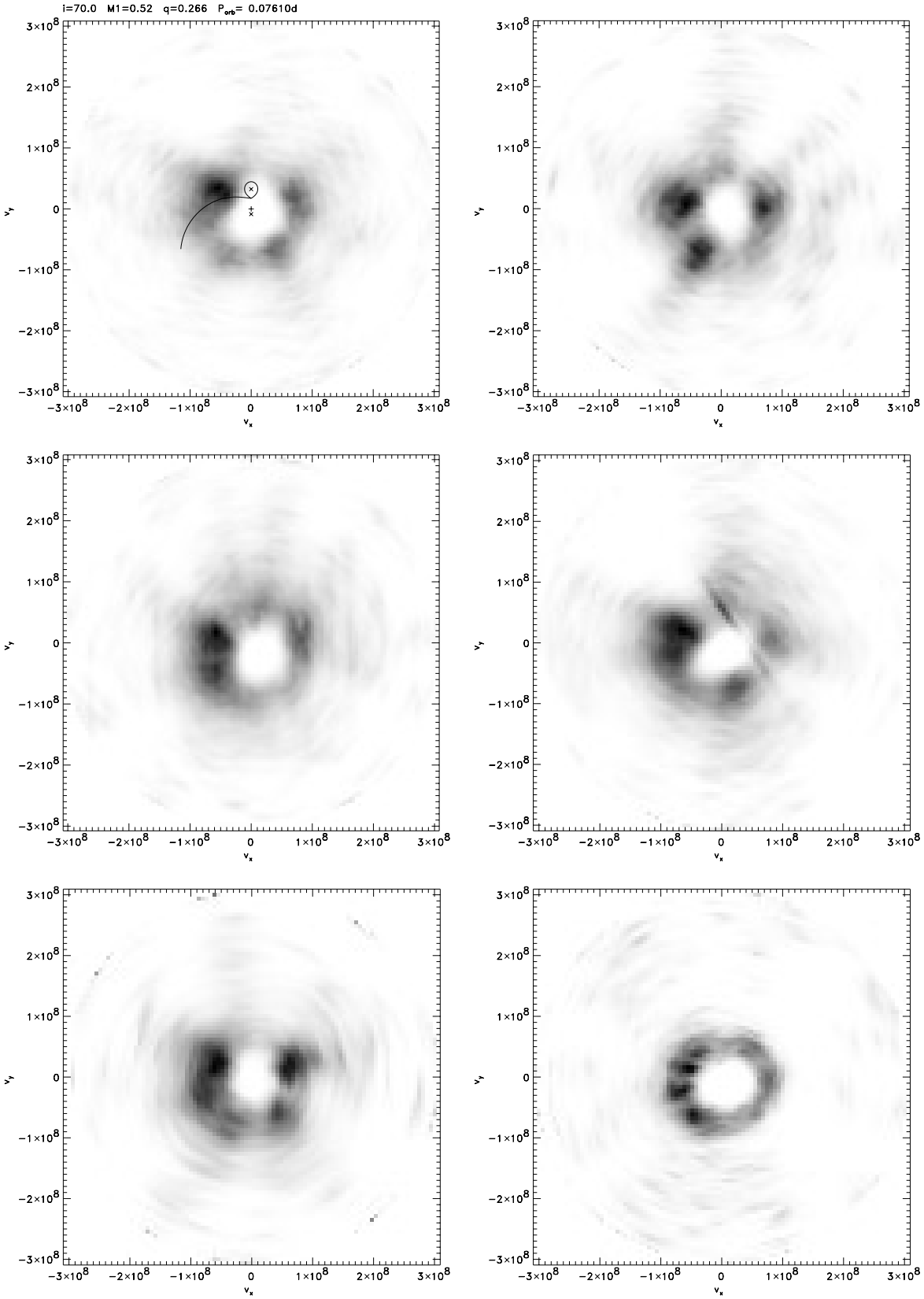

Fig. 14. Doppler maps of He I λ5876. The arrangement of the figures is same as that of Fig. 12.

References

Brett J.M., Smith R.C., 1993, MNRAS 264, 641
Bruch A., Steiner J.E., Gneiding C.D., 2000, PASP 112, 237
Hirose M., Osaki Y., 1990, PASJ 42, 135
Horne K., Wade R.A., Szkody P., 1986, MNRAS 219, 791
Houdebine E.R., Doyle J.G., Kościelecki M., 1995, A&A 294, 773
Kaitchuck R.H., Schlegel E.M., Honeycutt R.K., et al., 1994, ApJS 93, 519
Kato T., Haseda K., Takamizawa K., Kazarovets E.V., Samus N.N., 1998, IBVS No.4585
Marsh T.R., Horne K., 1988, MNRAS 235, 269
Osaki Y., 1989, PASJ 41, 1005
Satyvoldiev V., 1972, Astron. Tsirk. No.711
Satyvoldiev V., 1982, Perem. Zvezdy Pril. 4, 127
Schneider D.P., Young P., 1980, ApJ 238, 946
Shafter A.W., 1983, ApJ 267, 222
Shafter A.W., Szkody P., Thorstensen J.R., 1986, ApJ 308, 765
Smith R.C., 1990, In: Mauche C.W. (ed.) Accretion-Powered Compact Binaries. Cambridge University Press, p. 89
Spruit H.C., 1999, http://www.mpa-garching.mpg.de/∼henk/
Thorstensen J.R., 1999, IBVS No. 4749
Warner B., 1995, Cataclysmic Variable Stars. Cambridge University Press
Whitehurst R., 1988, MNRAS 232, 35
Whitehurst R., King A., 1991, MNRAS 249, 25